Time Scales of Variability of the Tropical Atmosphere Derived from Cloud-Defined Weather States

GEORGE TSELIOUDIS

Department of Applied Physics and Applied Mathematics, Columbia University, and NASA Goddard Institute for Space Studies, New York, New York, and Research Center for Atmospheric Physics and Climatology, Academy of Athens, Athens, Greece

WILLIAM B. ROSSOW

NOAA/CREST Center, The City College of New York, New York, New York

(Manuscript received 15 December 2009, in final form 16 September 2010)

ABSTRACT

The recent analysis of Rossow et al. used a clustering technique to derive six tropical weather states (WS) based on mesoscale cloud-type patterns and documented the spatial distribution of those WS and the modes of variability of the convective WS in the tropical western Pacific. In this study, the global tropics are separated into 30° × 30° regions, and a clustering algorithm is applied to the regional WS frequency distributions to derive the dominant modes of weather state variability (or the climate state variability) in each region. The results show that the whole tropical atmosphere oscillates between a convectively active and a convectively suppressed regime with the exception of the eastern parts of the two ocean basins, where the oscillation is between a stratocumulus and a trade cumulus regime. The dominant mode of both those oscillations is the seasonal cycle with the exception of the eastern Indian and western–central Pacific region, where El Niño frequencies dominate. The transitions between the convectively active and suppressed regimes produce longwave (LW) and shortwave (SW) top-of-atmosphere (TOA) radiative differences that are of opposite sign and of similar magnitude, being of order 20–30 W m^{-2} over ocean and 10–20 W m^{-2} over land and thus producing an overall balance in the TOA radiative budget. The precipitation differences between the convectively active and suppressed regimes are found to be of order 2.5–3 mm day^{-1} over ocean and 1–2.4 mm day^{-1} over land. Finally, the transitions between the stratocumulus and shallow cumulus regimes produce noticeable TOA SW differences of order 10–20 W m^{-2} and very small TOA LW and precipitation differences. The potential climate feedback implications of the regime radiation and precipitation differences are discussed.

1. Introduction

Tropical atmospheric variability has been studied extensively, revealing the dominance of the ENSO cycle in the tropical Pacific (e.g., Philander 1990; Koberle and Philander 1994), the presence of multiple scales of variability and the role of the coupled annual cycle in the tropical Atlantic (e.g., Neelin et al. 1998; Giannini et al. 2000), and the seasonal/monsoonal signals in the Indian Ocean and over the continental landmasses (e.g., Webster et al. 1998). Most of those studies are local in nature, with particular emphasis given to the western Pacific warm pool and the eastern Pacific stratocumulus regions. Furthermore, tropical atmospheric variability is usually derived from a single parameter, such as top-of-atmosphere (TOA) outgoing longwave radiation (OLR), sea surface temperature (SST), or the wind components. The regional focus of previous analyses and the fact that they resolve tropical processes through the use of single, relatively broad indicators makes it hard to synthesize them into a comprehensive description of the variability of the whole tropics and to quantify at planetary scales the changes in tropical cloud, radiation, and precipitation between the different modes of variability. Given that in a climate change situation, radiative and hydrologic feedbacks can result from subtle changes in the frequency of the primary variability regimes (e.g., Bony et al. 2006 and references therein), it is important to derive a global baseline of the cloud, radiation, and precipitation differences between the modes of tropical variability.

Corresponding author address: George Tselioudis, NASA GISS, Columbia University, 2880 Broadway, New York, NY 10025.
E-mail: gt9@columbia.edu

DOI: 10.1175/2010JCLI3574.1

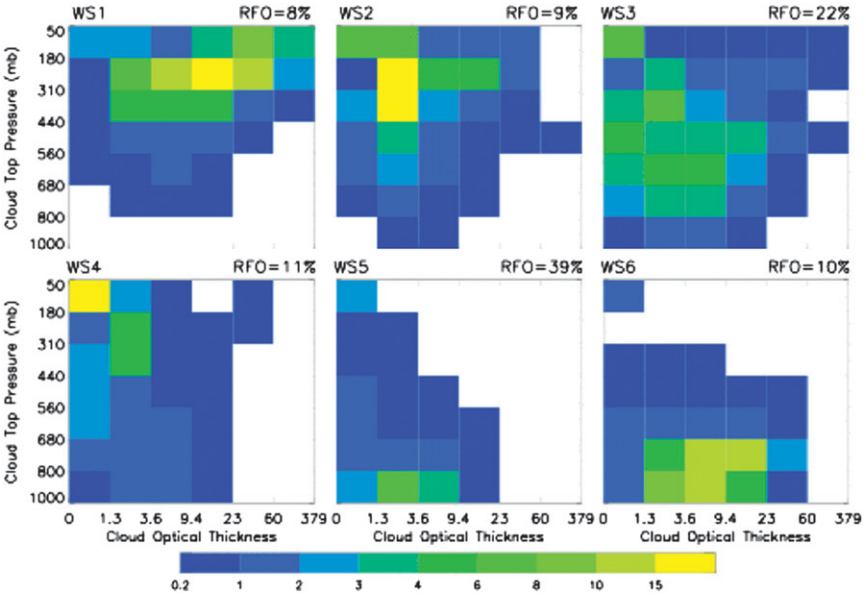

FIG. 1. The six TAU-PC frequency histogram patterns (WS) that best describe the 3-hourly variations of cloud properties in 2.5° latitude–longitude regions covering the whole tropics (15°S–15°N) for 21.5 yr (1983–2004) from ISCCP data. Each state is numbered (top left corner) from "most convectively active" to "least convectively active" and their relative frequency of occurrence (RFO) is shown in the top right corner. (From R05.)

The recent analysis of Rossow et al. (2005, hereafter R05) applied a clustering technique on International Satellite Cloud Climatology Project (ISCCP) cloud-type histograms to derive tropical weather states (WS) based on mesoscale cloud–type patterns that come from both the visible and infrared radiation signatures of the clouds. Six WS were derived, ranging from deep convective to shallow cumulus. R05 then examined the space distribution of the six WS over the global tropics and documented the modes of variability of the convective WS in the tropical western Pacific.

The analysis of R05 applied the clustering algorithm to 2.5° grid boxes and documented cloud type variability at the "cloud system" scale, where the cloud field is the result of the action of relatively fast processes with periods up to the intraseasonal scale. In the present study, cloud variability at basinwide regions is examined with an emphasis on slower processes, starting from the seasonal change and moving on to longer periods. The study uses the WS structures derived in R05 to examine the larger-scale organization of WS in space and time. Over basin-scale areas at each point in time, a multitude of such WS is present; the particular combination of WS determines the regional properties of the radiation and hydrologic budgets. Here we explore whether there exist preferred WS combinations that dominate the variability at regional scales by applying a cluster analysis technique to the regional frequency distribution of WS. The dominant combinations of WS in each region are then used to quantitatively document the changes of the radiation and precipitation fields between the different modes of variability.

2. Methodology

In R05 the *K*-means clustering algorithm (Anderberg 1973) is applied to cloud optical thickness–cloud-top pressure (TAU-PC) histograms derived daily for 2.5° grid boxes from 21 yr of ISCCP-D1 data (Rossow and Schiffer 1999). A semiempirical scheme is employed to determine the optimum number of clusters, and the TAU-PC histograms of each cluster are derived. The method identifies six major WS in the global tropics, which are shown here in Fig. 1. The first three WS are dominated by convective (WS1), anvil cirrus (WS2), and midlevel (WS3) clouds and are characterized by R05 as convectively active. The other three WS are dominated by thin cirrus (WS4), shallow cumulus (WS5), and stratocumulus (WS6) clouds and are characterized as convectively suppressed.

In the present study, the tropics are separated into 30° × 30° regions (from 15°S to 15°N and every 30° of longitude starting from the Greenwich meridian), and daily a six-element vector is constructed for each region from the frequency of occurrence (FOC) of the six WS. Then the *K*-means clustering algorithm is applied to

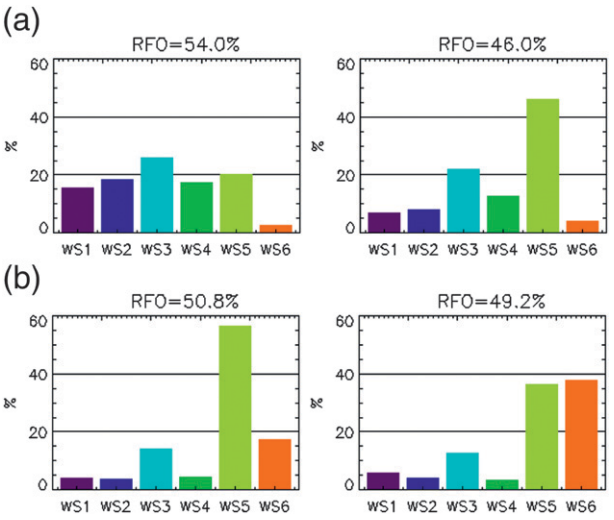

FIG. 2. (a) Frequency distribution of the six WS for the 120°–150°E region and for the (left) convectively active and (right) convectively suppressed CSs. (b) As in Fig. 1a, but for the 240°–270°E region and for the (left) shallow cumulus and (right) stratocumulus CSs.

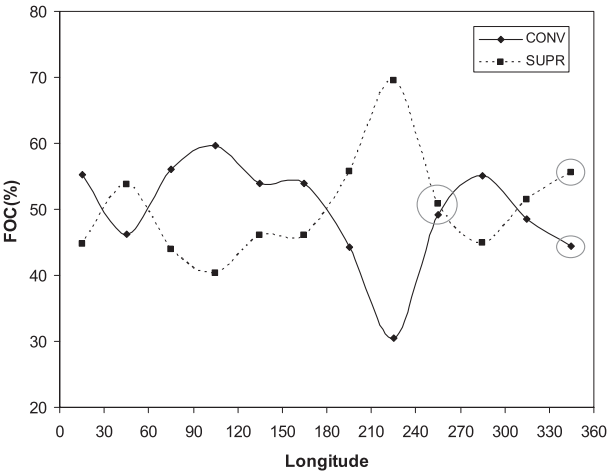

FIG. 3. Frequency of occurrence (FOC) of the convectively active and suppressed CSs. In two regions marked with circles, the CSs are the stratocumulus and shallow cumulus ones, respectively.

those six-element vectors for the 21-yr period to derive the dominant modes of weather state variability in each region. Increasing numbers of clusters are tested in the clustering calculations, and the semiempirical method described in R05 is applied to determine the ultimate cluster number. The method applies pattern correlation criteria to accept or reject additional clusters depending on their similarity with existing ones. It is found that for all regions, two main clusters describe the dominant modes of WS variability, and those two clusters are hereafter referred to as climate states (CS). Once the main CS for all tropical regions are derived, the ISCCP radiative flux dataset (ISCCP-FD) (Zhang et al. 2004) and the Global Precipitation Climatology Project (GPCP) dataset (Huffman et al. 2001) are used to calculate the radiation and precipitation properties of each CS.

It is important to note here that the choice of examining 30°-wide regions at daily time scales filters out higher-frequency variability caused by the propagation of tropical waves with small spatial extents. This is done because the emphasis of the present work is on seasonal and interannual rather than intraseasonal or shorter time scales. Also, the 21-yr duration of the dataset excludes the examination of variability with decadal or longer periods.

3. Results

The application of the *K*-means clustering algorithm to the WS distribution provided two CS for each 30°-wide tropical region. Figure 2a shows the two CSs for the 120°–150°E region located in the western Pacific. One CS (left panel) includes high percentages of the convectively active weather states (particularly the deep convective WS1 and the thick anvil WS2) and is therefore referred to as the convectively active CS, while the other CS (right panel) is dominated by a very high percentage of the shallow cumulus WS5 and is referred to as the convectively suppressed CS. The convectively active CS occurs 54% of the time, while the convectively suppressed CS occurs 46% of the time. This picture, with one CS that includes higher percentages of convectively active WS and a second CS with very high percentages of the shallow cumulus WS5, is observed with small deviations in ten out of twelve 30° regions of the global tropics. In the other two regions, located off the western coasts of South America and Africa, the two main CS include one CS that is dominated by shallow cumulus clouds (WS5) and a second CS that includes roughly equal amounts of stratocumulus (WS6) and shallow cumulus clouds. This is shown in Fig. 2b, where the two CS for the 240°–270°E region located off the western coast of South America are shown. The difference between the two CS is in the relative amounts of stratocumulus and shallow cumulus clouds, while the convective WS are relatively rare and roughly the same in the two CS. The shallow cumulus CS (left panel) occurs 50.8% of the time, while the stratocumulus CS occurs 49.2% of the time.

Figure 3 shows the frequency of occurrence of the convectively active and the convectively suppressed CS for all tropical regions. Note that in two regions (240°–270°E and 330°E–360°, marked with circles), the convectively active and suppressed regimes are replaced by the stratocumulus and shallow cumulus ones, respectively.

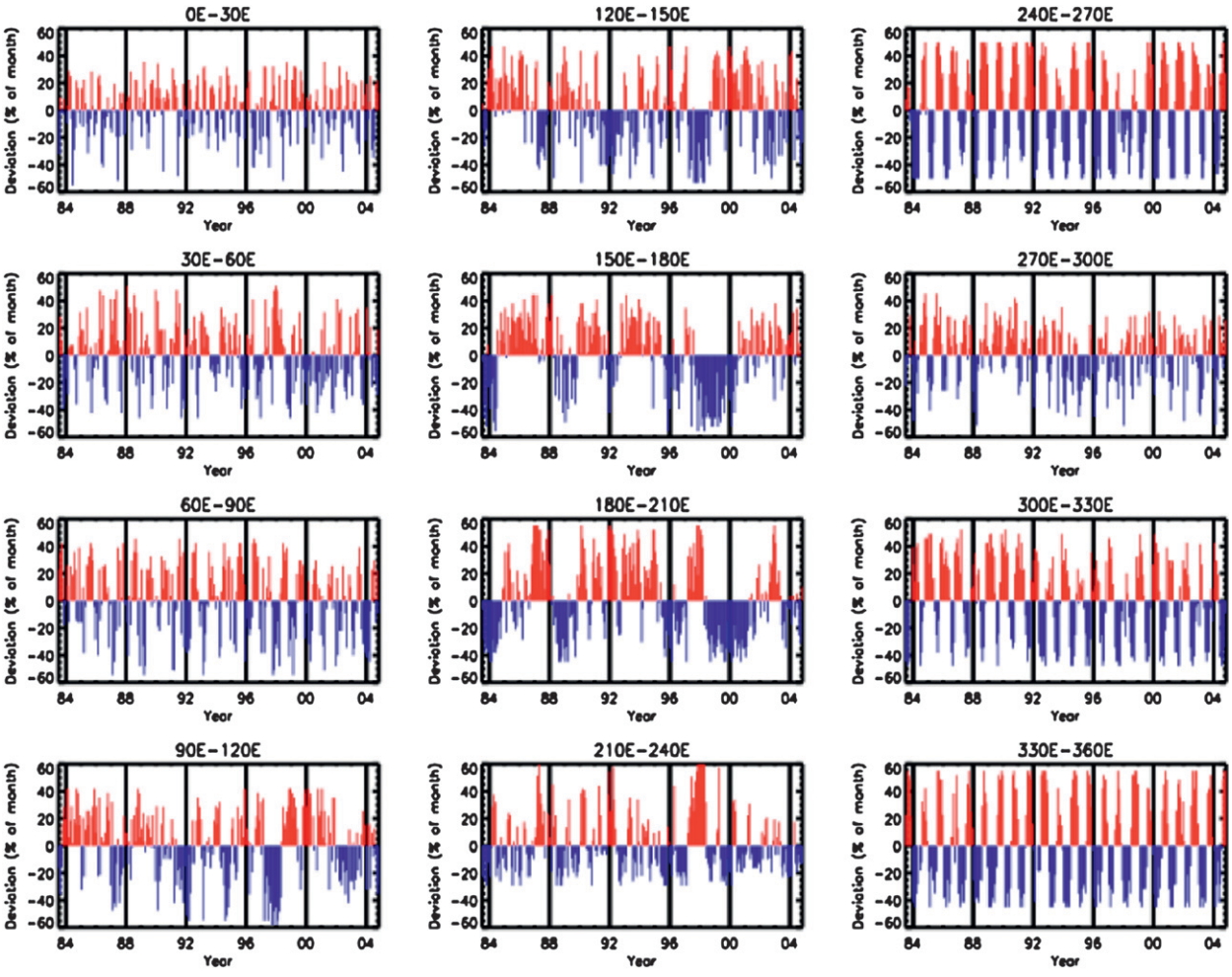

FIG. 4. Time series of the FOC of the convectively active CSs plotted as percent anomalies from the monthly-mean FOC, for all tropical regions and for the period from July 1983 to December 2004.

The convectively active regime is more frequent in the Indian Ocean–western Pacific region with about a 60% FOC, while the convectively suppressed regime is more frequent in the central Pacific (~70% FOC). In the rest of the tropics, the frequencies of the two regimes are rather similar and range between 45% and 55%.

To explore the time scales of variability of the derived CS, time series of the frequency of occurrence of each CS during 1-month intervals are calculated and plotted as percent anomalies from the monthly-mean frequency of occurrence of each CS. Figure 4 shows the time series of the convectively active regime for all tropical regions and for the period from July 1983 to December 2004. Two main regimes of variability can be observed in these plots. In the eastern Indian and western-central Pacific regions, the convectively active and suppressed CS alternate between El Niño and La Niña periods, with the convectively active regime becoming less frequent in the western Pacific and more frequent in the central Pacific during El Niño years (e.g., 1992, 1998). In all other regions of the tropics, both the convectively active and suppressed CSs and the stratocumulus and shallow cumulus CS alternate with very regular annual cycles. Note that in the 0°–30°E region and to a lesser degree in the 30°–60°E and 270°–300°E regions, the annual cycle is not as robust and appears to be modulated by a semi-annual signal. This is because those regions include roughly equal percentages of land and ocean surface that exhibit seasonal variability with different phases.

To quantify the major time scales of regional variability of the CS, wavelet analyses of the time series of CS are performed in all tropical regions. The wavelets provide the power spectra for the period from 1983 to 2004. The wavelet spectra for all twelve 30°-wide tropical regions confirm that the eastern–central Pacific variability is dominated by El Niño frequencies of 5–6 years

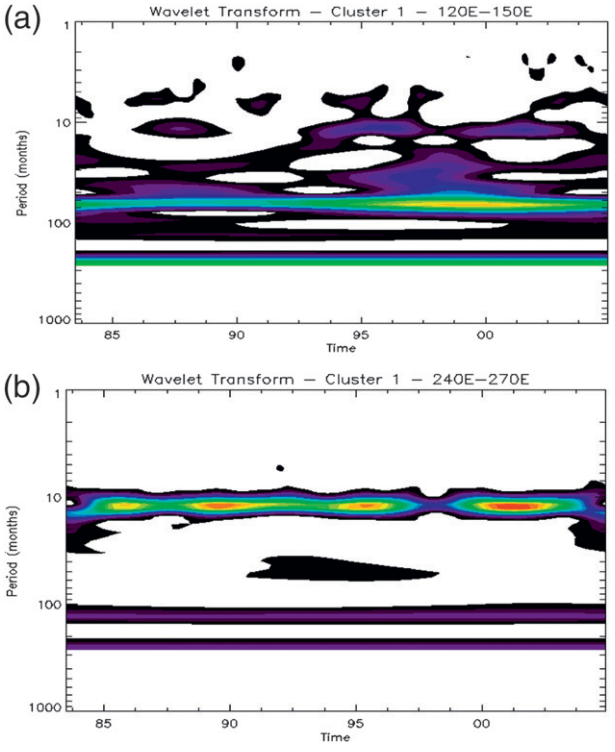

FIG. 5. Wavelet analysis results showing the dominant time scales of variation as a function of the year for (a) the convectively active CS for the western Pacific region (120°–150°E) and (b) the stratocumulus CS for the eastern Atlantic region (240°–270°E).

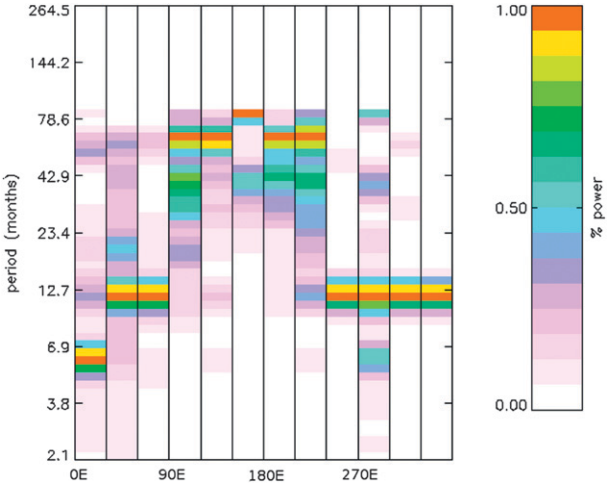

FIG. 6. Time-averaged wavelet frequencies for the whole tropics derived from averaging the wavelet power spectra of each 30° × 30° region over the period from July 1983 to December 2004. The result for each region is plotted as a percent power difference from the maximum power value. The period of maximum power for each region has a percent power value of 1.

with a weak annual cycle signal that is more pronounced in the latter part of the period, while the rest of the tropical variability is dominated by an annual signal that is strong throughout the 21-yr period. This result is partially demonstrated in Fig. 5, where the wavelet spectra for the 120°–150°E (top) and the 240°–270°E (bottom) regions are plotted. The figure shows the El Niño dominance and the weak annual cycle in the latter part of the season in the power spectrum of the western Pacific region, and the seasonal dominance in the power spectrum of the eastern Atlantic region.

To summarize the variability over the whole tropics, the power spectra for each region are averaged over time and the time-averaged wavelet frequencies are plotted in Fig. 6 as percent power differences from the maximum value. The plot then shows the period of maximum power (percent value of 1) and the strength relative to that of the power values at other periods. It can be seen from Fig. 6 that the maximum power of the tropical CS variability is at the 1-yr period in most regions, with the exception of the region between 90° and 240°E, where the maximum power is at periods of 5–6 years. Lower-frequency signals are present in areas outside the western–central Pacific (particularly in the regions of Africa and western South America), but the annual cycle signal is consistently dominant in those regions. It is important to note that even in the same basin, the annual cycle signal can be coming from entirely different processes. In the tropical Atlantic, for example, in the western part of the basin, the signal is achieved through seasonal transitions between the convectively active and suppressed CS, while in the eastern part it is achieved through seasonal transitions between the stratocumulus and shallow cumulus CS.

The CS structures derived above are used next to explore the differences in the radiation and precipitation budgets between the two phases of the CS oscillations. For all periods that a particular CS is present in a region, the radiation and precipitation data are averaged and then the differences in the average values of the two CS are calculated. Figure 7a shows the difference in TOA longwave (LW) and TOA shortwave (SW) radiative flux components between the convectively active/stratocumulus and the convectively suppressed/shallow cumulus CS in all tropical regions. The El Niño–driven transitions between the convectively active and suppressed CS in the eastern Indian Ocean and the western Pacific produce TOA LW differences of order 20–30 W m^{-2}. The seasonally driven transitions between those two CS produce in the central Indian and the western Atlantic Oceans TOA LW differences of order 20–25 W m^{-2} and over the continents of Africa and South America differences of order 10–20 W m^{-2}. The seasonally driven transitions between the stratocumulus and shallow cumulus CS produce TOA LW

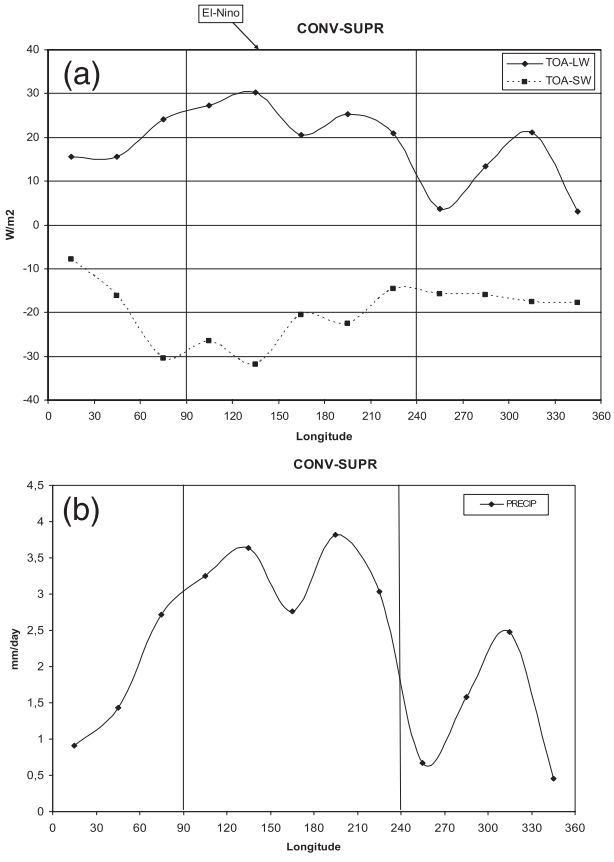

FIG. 7. (a) Differences in TOA LW (top line) and TOA SW (bottom line) radiative fluxes between the convectively active/stratocumulus and the convectively suppressed/shallow cumulus CSs in all 30° × 30° tropical regions. (b) As in Fig. 4a, but for differences in precipitation.

differences of less than 5 W m^{-2}. In the TOA SW fluxes, the transitions between the convectively active and suppressed CSs in the Indian Ocean and western Pacific regions produce differences of 20–30 W m^{-2}, while the seasonal transitions in all other regions produce differences of 10–20 W m^{-2}. The exception is the 210°–240°E region in the central Pacific, where the presence of a high percentage of stratocumulus clouds in the convectively suppressed CS results in TOA SW differences between the two CS of only about 15 W m^{-2}.

The differences in precipitation between the convectively active/stratocumulus and the convectively suppressed/shallow cumulus regimes in Fig. 7b show longitudinal features similar to those of the TOA LW field. The El Niño–driven transitions between the convectively active and suppressed CS in the eastern Indian Ocean and the western Pacific produce precipitation differences of 2.5–4 mm day^{-1}. The seasonally driven transitions between those two CS produce in the central Indian and the western Atlantic Oceans precipitation differences of 2.5–3 mm day^{-1} and over the continents of Africa and South America differences of 1–2.5 mm day^{-1}. The seasonally driven transitions between the stratocumulus and shallow cumulus CSs produce small precipitation differences of less than 1 mm day^{-1}.

4. Summary and discussion

The results presented here show that the whole tropical atmosphere oscillates between a convectively active and a convectively suppressed regime with the exception of the eastern parts of the two ocean basins, where the oscillation is between a stratocumulus and a trade cumulus regime. The dominant mode of both those oscillations is the seasonal cycle with the exception of the eastern Indian and western–central Pacific regions, where El Niño frequencies dominate. The transitions between the convectively active and suppressed regimes produce LW and SW TOA radiative differences that are of opposite sign and of similar magnitude, being of order 20–30 W m^{-2} over ocean and 10–20 W m^{-2} over land, and thus producing an overall balance in the TOA radiative budget. This TOA balance, however, can be deceiving, as the SW signal manifests itself at the surface radiative budget, while the LW signal manifests itself at the budget of the atmospheric column. This implies that the two TOA radiative signals of similar magnitude apply different forcings to the atmospheric and oceanic circulations. The precipitation differences between the convectively active and suppressed regimes are found to be of order 2.5–3 mm day^{-1} over ocean and 1–2.4 mm day^{-1} over land. Finally, the transitions between the stratocumulus and shallow cumulus regimes produce noticeable TOA SW differences of order 10–20 W m^{-2} and very small TOA LW and precipitation differences.

It is important to note that the time variability signals in this study are derived from the mean properties of the cloud field in 30° × 30° boxes centered on the equator. Any latitudinal or longitudinal cloud shifts within the boxes would produce a spectral imprint only if they altered the mean properties of the clouds in the box. It is well known that the ITCZ exhibits seasonal latitudinal shifts around the globe (e.g., Chao and Chen 2001; Hu et al. 2007). Hu et al. (2007) show in their Fig. 2 that for the 20°S–20°N latitude zone, those shifts produce pronounced seasonal asymmetries in most locations, with the exception of the western and central Pacific, where the regular seasonal progression of a uniform ITCZ structure produces small seasonal asymmetries in the zone. This explains the fact that the wavelet analysis shown in Fig. 5 of this paper does not produce a seasonal signal but only El Niño peaks in the

western–central Pacific region. The seasonally asymmetrical ITCZ migrations shown in Hu et al. (2007) can also explain the seasonal signal in all locations of convectively active-to-suppressed CS transitions, especially if one considers the theory proposed by Chao and Chen (2001) that even monsoonal circulations can be attributed to ITCZ migrations.

The tropical regime differences shown in Fig. 7 are particularly important in relation to radiative and hydrologic feedbacks that could result from changes in El Niño frequency or changes in the stratocumulus–shallow cumulus transition with climate warming. The near cancellation of the SW and LW regime differences in the El Niño–dominated region would imply a small TOA signal from an El Niño frequency change. This cancellation, however, must be viewed with caution given the different forcing manifestations of the two radiative components noted above. On the other hand, the imbalance in the TOA radiative components of the stratocumulus-to-shallow cumulus transition and the dominance of the SW component explains in part the emphasis that is given to this transition in climate feedback studies. The results of the present study provide a quantitative baseline for the radiation and precipitation changes between the major tropical climate regimes. This baseline can be used as an additional constraint for climate model evaluation that will judge the ability of the models to correctly simulate the effects of shifts in the frequency of those climate regimes.

Acknowledgments. We thank Alison Sheffield for her valuable contribution in implementing the clustering diagnostics. We also thank an anonymous reviewer for thorough and constructive comments. Work by G. T and W. B. R was supported by the NASA Modeling and Analysis Program (managed by Dr. David Considine) under Grants 08MAP0004 and NNXD7AN04G.

REFERENCES

Anderberg, M. R., 1973: *Cluster Analysis for Applications*. Elsevier, 359 pp.

Bony, S., and Coauthors, 2006: How well do we understand and evaluate climate change feedback processes? *J. Climate,* **19,** 3445–3482.

Chao, W. C., and B. Chen, 2001: The origin of monsoons. *J. Atmos. Sci.,* **58,** 3497–3507.

Giannini, A., Y. Kushnir, and M. A. Cane, 2000: Interannual variability of Caribbean rainfall, ENSO, and the Atlantic Ocean. *J. Climate,* **13,** 297–311.

Hu, Y., D. Li, and J. Liu, 2007: Abrupt seasonal variation of the ITCZ and the Hadley circulation. *Geophys. Res. Lett.,* **34,** L18814, doi:10.1029/2007GL030950.

Huffman, G. J., R. F. Adler, M. Morrissey, D. T. Bolvin, S. Curtis, R. Joyce, B. McGavock, and J. Susskind, 2001: Global precipitation at one-degree daily resolution from multisatellite observations. *J. Hydrometeor.,* **2,** 36–50.

Koberle, C., and S. G. H. Philander, 1994: On the processes that control seasonal variations of sea surface temperature in the tropical Pacific Ocean. *Tellus,* **46A,** 481–496.

Neelin, J. D., D. S. Battisti, A. C. Hirst, F.-F. Jin, Y. Wakata, T. Yamagata, and S. E. Zebiak, 1998: ENSO theory. *J. Geophys. Res.,* **103,** 14 261–14 290.

Philander, S. G. H., 1990: *El Niño, La Niña, and the Southern Oscillation*, International Geophysics Series, Vol. 46, Academic Press, 293 pp.

Rossow, W. B., and R. A. Schiffer, 1999: Advances in understanding clouds from ISCCP. *Bull. Amer. Meteor. Soc.,* **80,** 2261–2288.

——, G. Tselioudis, A. Polak, and C. Jakob, 2005: Tropical climate described as a distribution of weather states indicated by distinct mesoscale cloud property mixtures. *Geophys. Res. Lett.,* **32,** L21812, doi:10.1029/2005GL024584.

Webster, P. J., V. O. Magaña, T. N. Palmer, J. Shukla, R. A. Tomas, M. Yanai, and T. Yasunari, 1998: Monsoons: Processes, predictability, and the prospects of prediction. *J. Geophys. Res.,* **103,** 14 451–14 510.

Zhang, Y., W. B. Rossow, A. A. Lacis, V. Oinas, and M. I. Mishchenko, 2004: Calculation of radiative fluxes from the surface to top of atmosphere based on ISCCP and other global data sets: Refinements of the radiative transfer model and the input data. *J. Geophys. Res.,* **109,** D19105, doi:10.1029/2003JD004457.